Origin of extra capacity in the solid electrolyte interphase near high-capacity iron carbide anode for Li ion batteries

Dongjiang Chen[1], Chao Feng[1], Yupei Han[1], Bo Yu[1], Wei Chen[1], Ziqi Zhou[1], Ning Chen[1], John B. Goodenough[2], Weidong He[1,3]★

[1]School of Physics, University of Electronic Science and Technology of China, Chengdu 611731, China

[2]Materials Science and Engineering Program & Texas Materials Institute, The University of Texas at Austin, Austin TX 78712, USA

[3]National Key Laboratory of Science and Technology on Advanced Composites in Special Environments, and Center for Composite Materials and Structures, Harbin Institute of Technology, Harbin 150080, China

E-mail: *weidong.he@uestc.edu.cn*

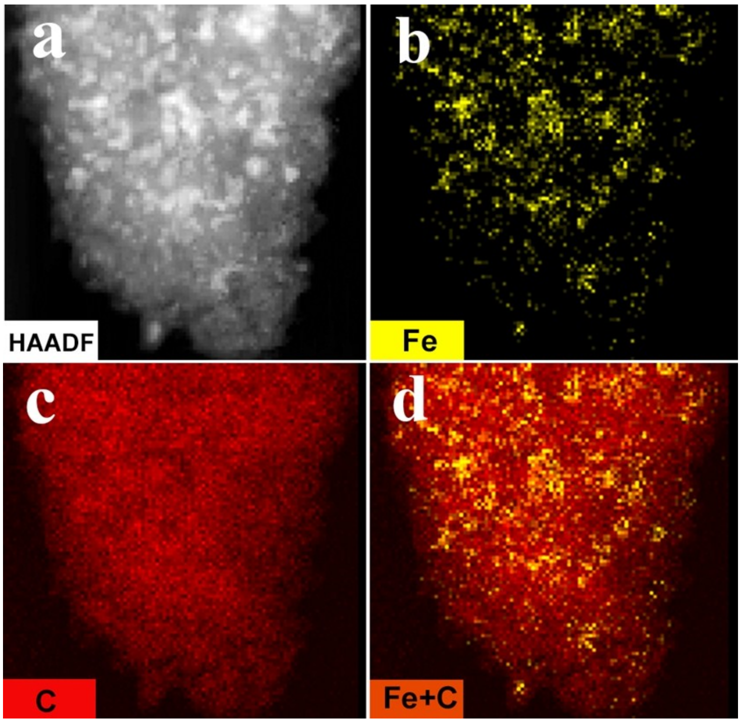

Supplementary Figure 1 | a-d, TEM image and the corresponding mapping images of core-shell $C@Fe_3C/Fe$ powders.

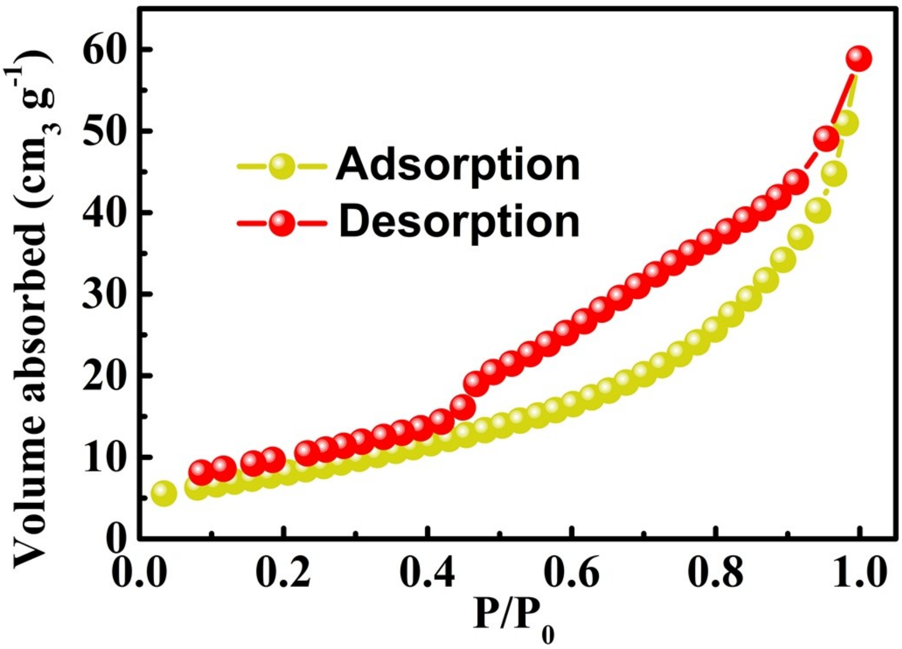

Supplementary Figure 2 | N_2 adsorption/desorption isotherm of the core-shellC@Fe_3C/Fe powders.

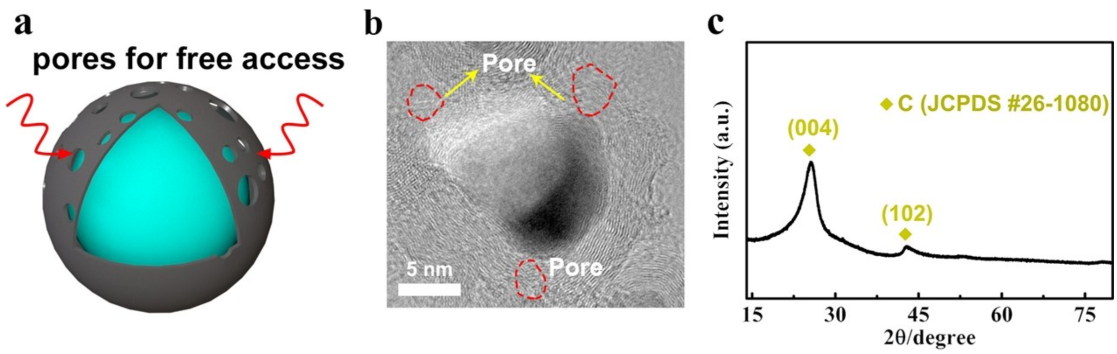

Supplementary Figure 3 | a, Schematics of the porous core-shell architecture. **b,** TEM image of the C@Fe_3C/Fe nanoparticle. **c,** XRD pattern of the carbonaceous powders after removing iron species from C@Fe3C/Fe powders.

The calculations of Fe and Fe_3C mass contents in C@Fe_3C/Fe nanoparticles based on TGA analysis are as follows:

$$4Fe + 3O_2 = 2Fe_2O_3 \quad (S1)$$

$$4Fe_3C + 13O_2 = 6Fe_2O_3 + 4CO_2 \quad (S2)$$

$$m_{Fe}\,(\%) = \frac{2}{3} \times m_O(\%) \times \frac{M_{Fe}}{M_O} \quad (S3)$$

$$m_{Fe2O_3}{}'\,(\%) = \frac{1}{3} \times m_O\,(\%) \times \frac{M_{Fe_2O_3}{}'}{M_o} \quad (S4)$$

$$m_{Fe3C}(\%) = \frac{2}{3} \times \left(m_{Fe_2O_3} - m_{Fe_2O_3}{}'\right)(\%) \times \frac{M_{Fe_3C}}{M_{Fe_2O_3}} \quad (S5)$$

where $m_O\,(\%)$ of 6 wt. % is the weight increase in the range of 190 °C ~ 410 °C, which is attributed to oxygen from the change of Fe to Fe_2O_3. $m_{Fe}\,(\%)$ is the mass percentage of Fe nanoparticles in the C@Fe_3C/Fe compound. $m_{Fe_2O_3}\,(\%)$ of 43 wt. % is the total mass of Fe_2O_3 arising from Fe and Fe_3C together when the temperature is raised at 900 °C. $m_{Fe_2O_3}{}'\,(\%)$ is the mass percentage of Fe_2O_3, as calculated based on Equation (S1). $m_{Fe_3C}\,(\%)$ is the mass percentage of Fe_3C in C@Fe_3C/Fe nanoparticles. M_{Fe}, M_O, $M_{Fe_2O_3}$and M_{Fe_3C} are the molar masses of Fe, O, Fe_2O_3 and Fe_3C. As a result, the Fe and Fe_3C contents in the composite are 14 wt. % and 17 wt. %, respectively.

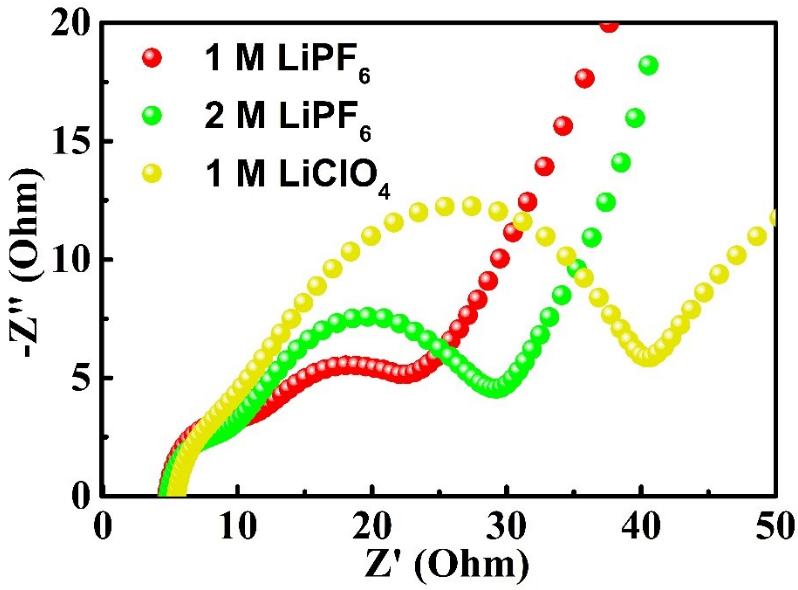

Supplementary Figure 4 | Post-cycle EIS of batteries with 1 M $LiPF_6$, 2 M $LiPF_6$ and 1 M $LiClO_4$ electrolytes.

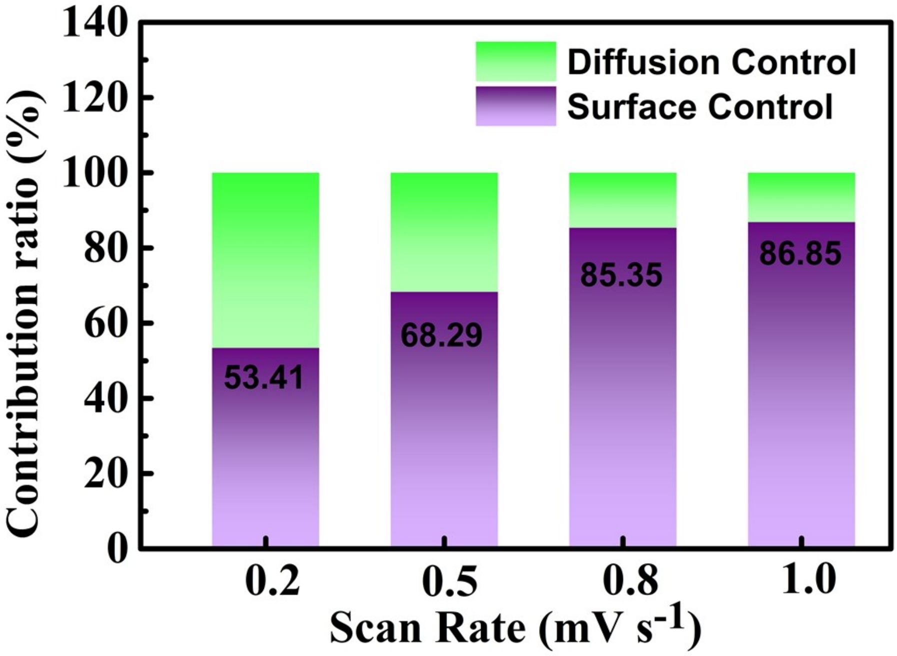

Supplementary Figure 5 | Current response of C@Fe_3C/Fe nanoparticles at various scan rates.

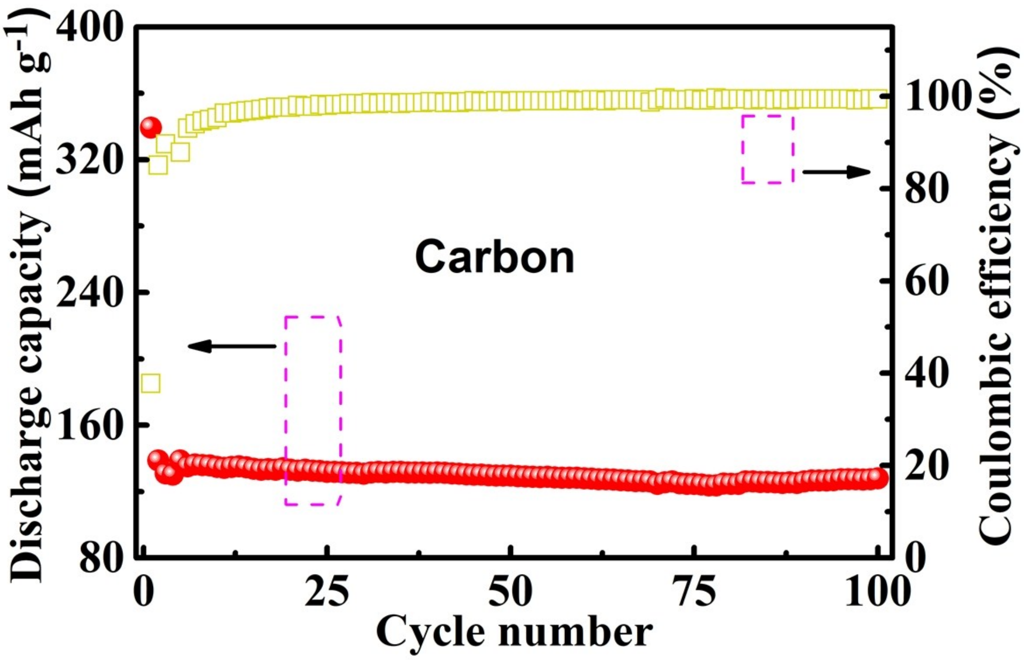

Supplementary Figure 6 | Cycling performances and Columbic efficiencies of carbon anode with 1 M LiFP6 with a current density of 1 A g^{-1}.

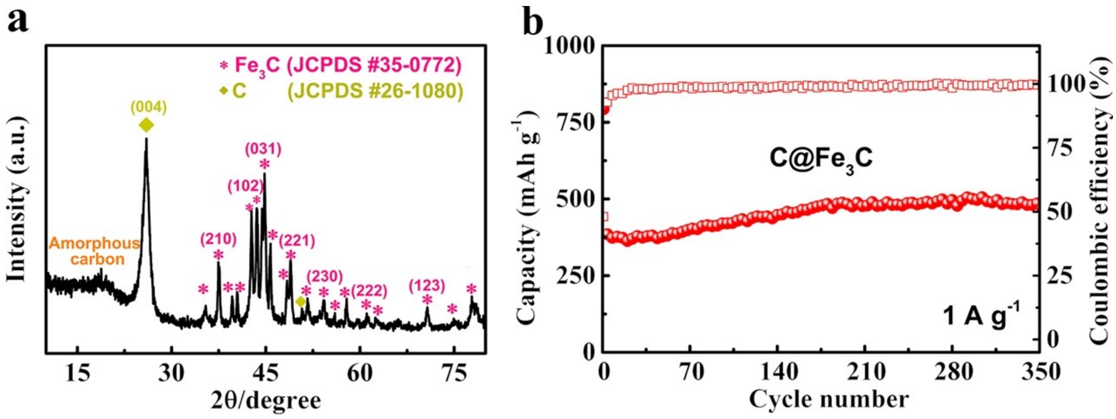

Supplementary Figure 7 | a, XRD patterns and **b,** Cyclic performance of C@Fe_3C anode.

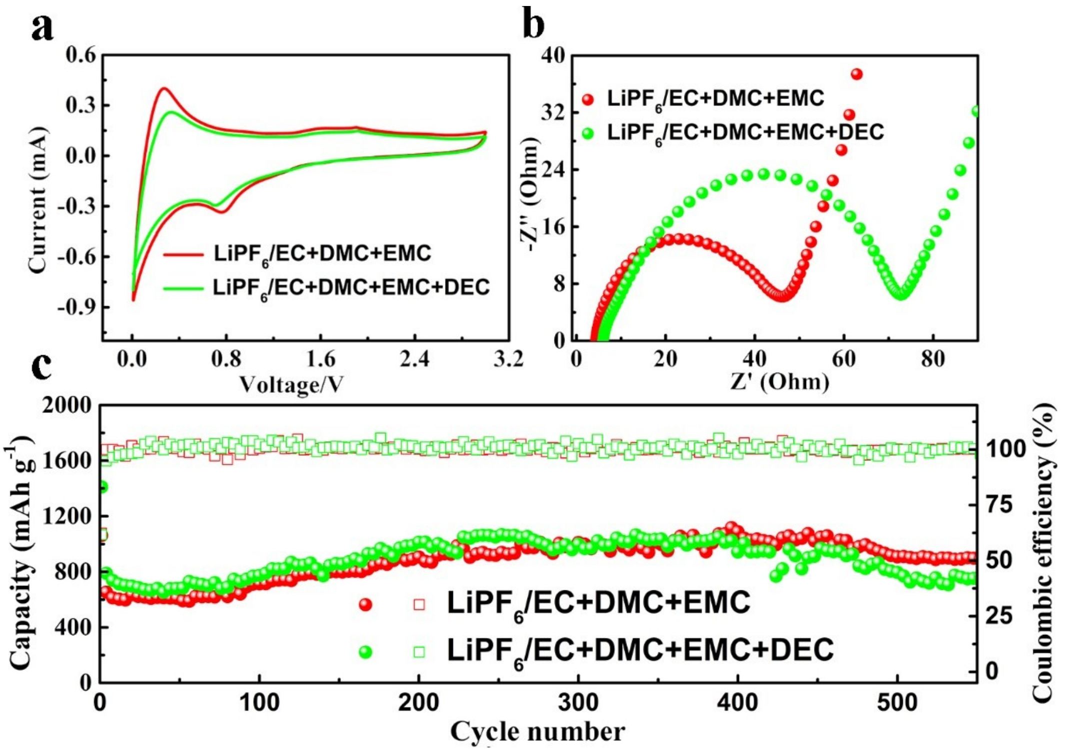

Supplementary Figure 8 | a, CV curves (recorded at 0.5 mV/s). **b,** EIS curves (recorded at 0.10 Hz to 1.0 MHz) and **c,** cycle performances (recorded at 1 A g^{-1}) of the C@Fe_3C/Fe anode with 1 M $LiFP_6$/EC+DMC+EMC electrolyte and 1 M $LiFP_6$/EC+DMC+EMC+DEC electrolyte.

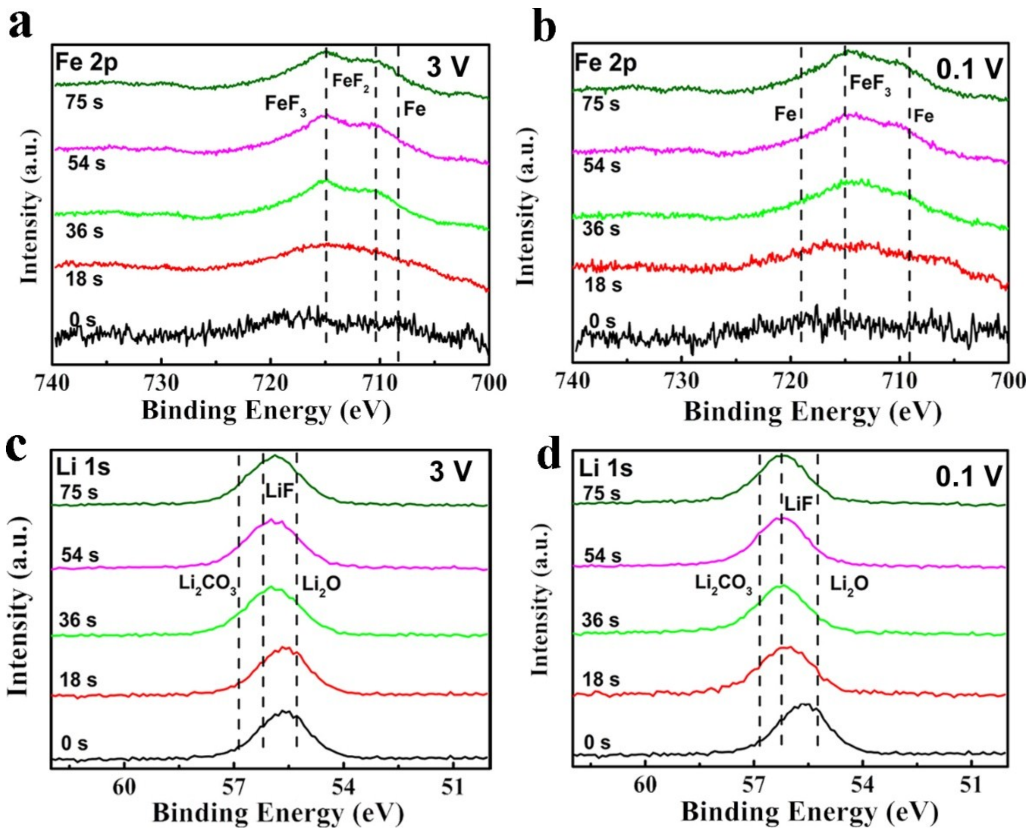

Supplementary Figure 9 | a, b Fe 2p and **c, d** Li 1s XPS spectra of the SEI on C@Fe_3C/Fe anode after various etching times at 3 V and 0.1 V, respectively (the surface at 0 s).

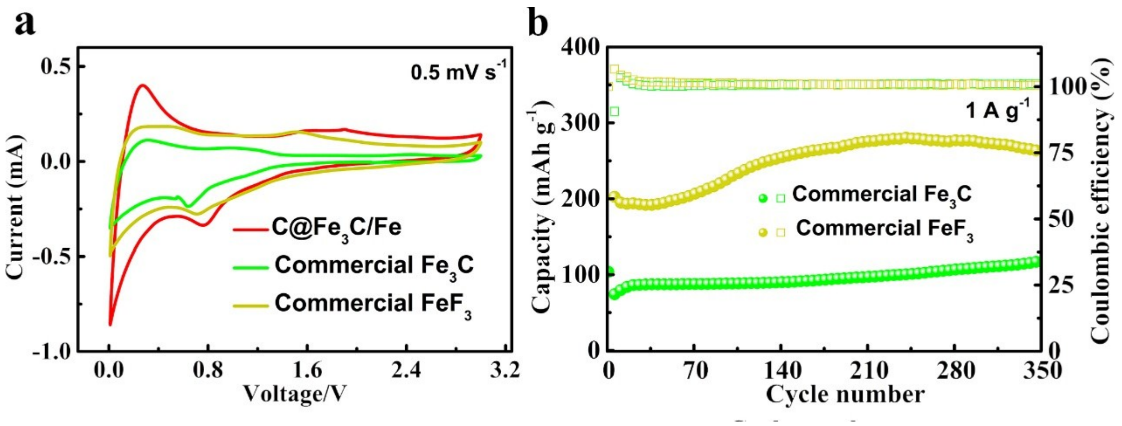

Supplementary Figure 10 | a, CV curves at 0.5 mV/s and **b,** Cyclic performances and Columbic efficiencies of commercial Fe_3C and FeF_3 electrodes at a current density of 1 A g^{-1}.

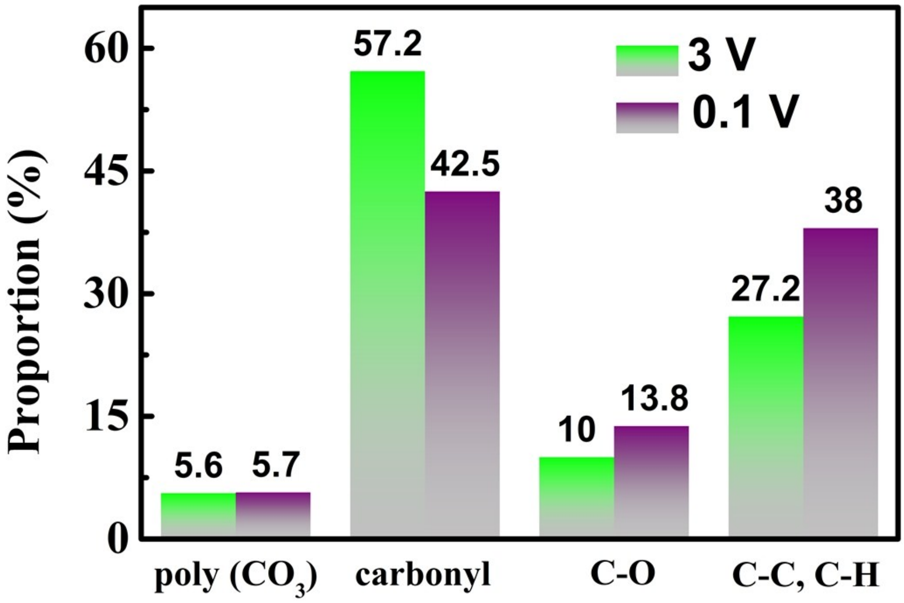

Supplementary Figure 11 | The variation of the SEI composition during the electrochemical reactions.

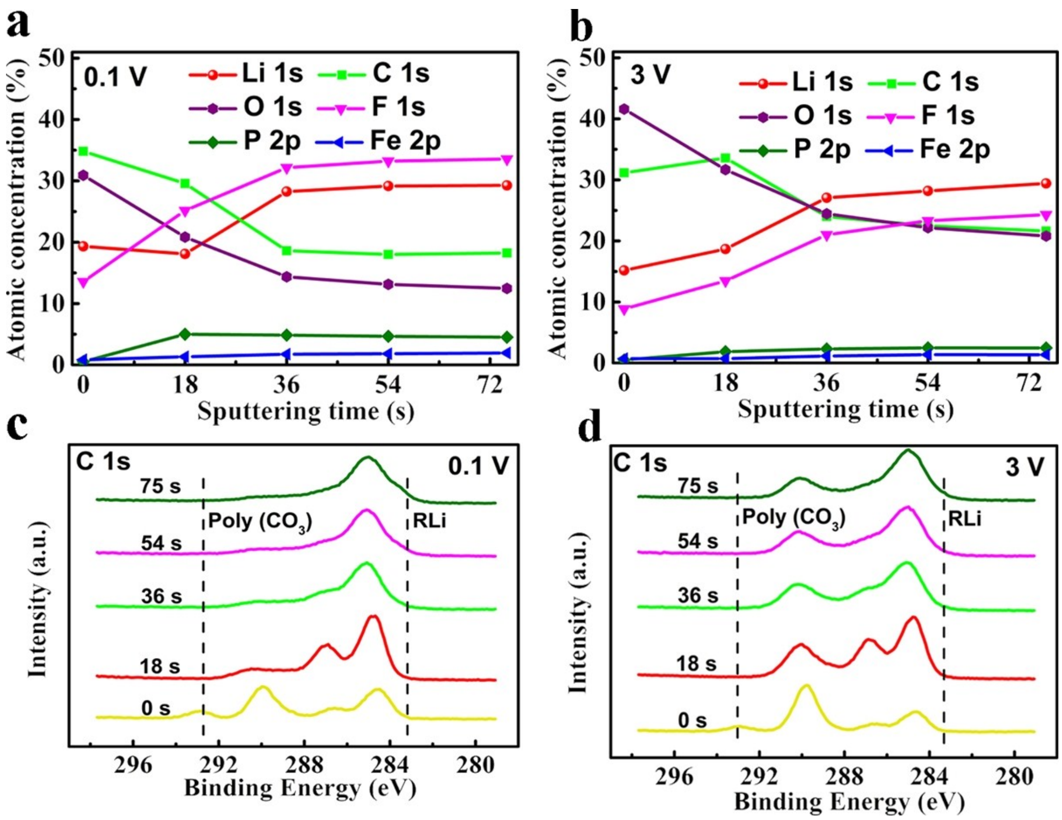

Supplementary Figure 12 | a, b Depth profiles of the XPS spectra for the core-shellC@Fe_3C/Fe at 0.1 V and 3 V. **c, d** The C 1s XPS spectra of the SEI in 1 M $LiPF_6$/EC+DMC+EMC electrolyte after various etching times at 0.1 V and 3 V, respectively (the surface at 0 s).

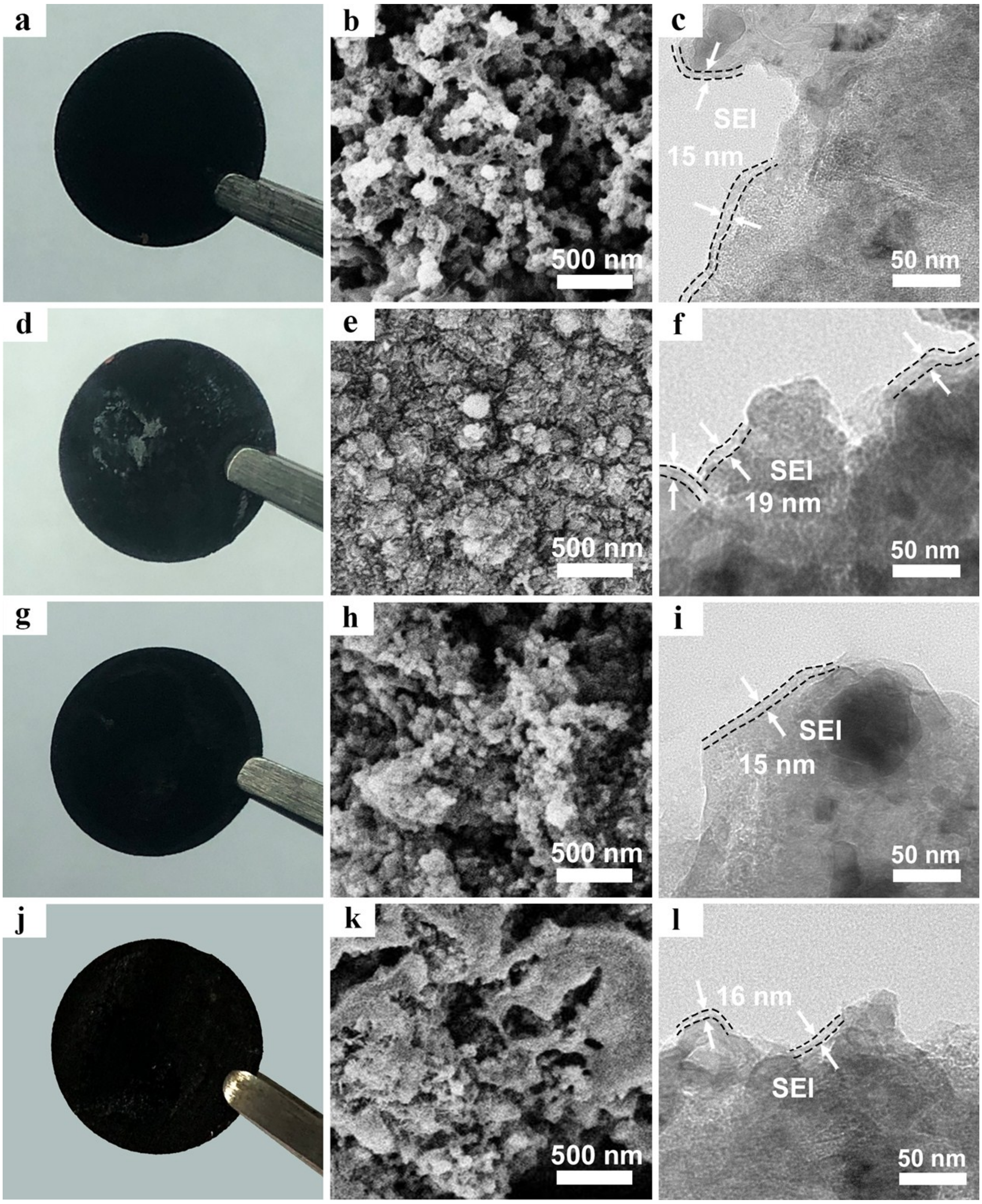

Supplementary Figure 13 | Digital photos, SEM and TEM images of the post-cycle C@Fe_3C/Fe anodes with **a-c,** 1 M $LiPF_6$/EC+DMC+EMC electrolyte, **d-f,** 2 M $LiPF_6$/EC+DMC+EMC electrolyte, **g-i,** 1 M $LiClO_4$/EC+DMC+EMC electrolyte and **j-l,** 1 M $LiPF_6$/EC+DMC+EMC+DEC electrolyte.

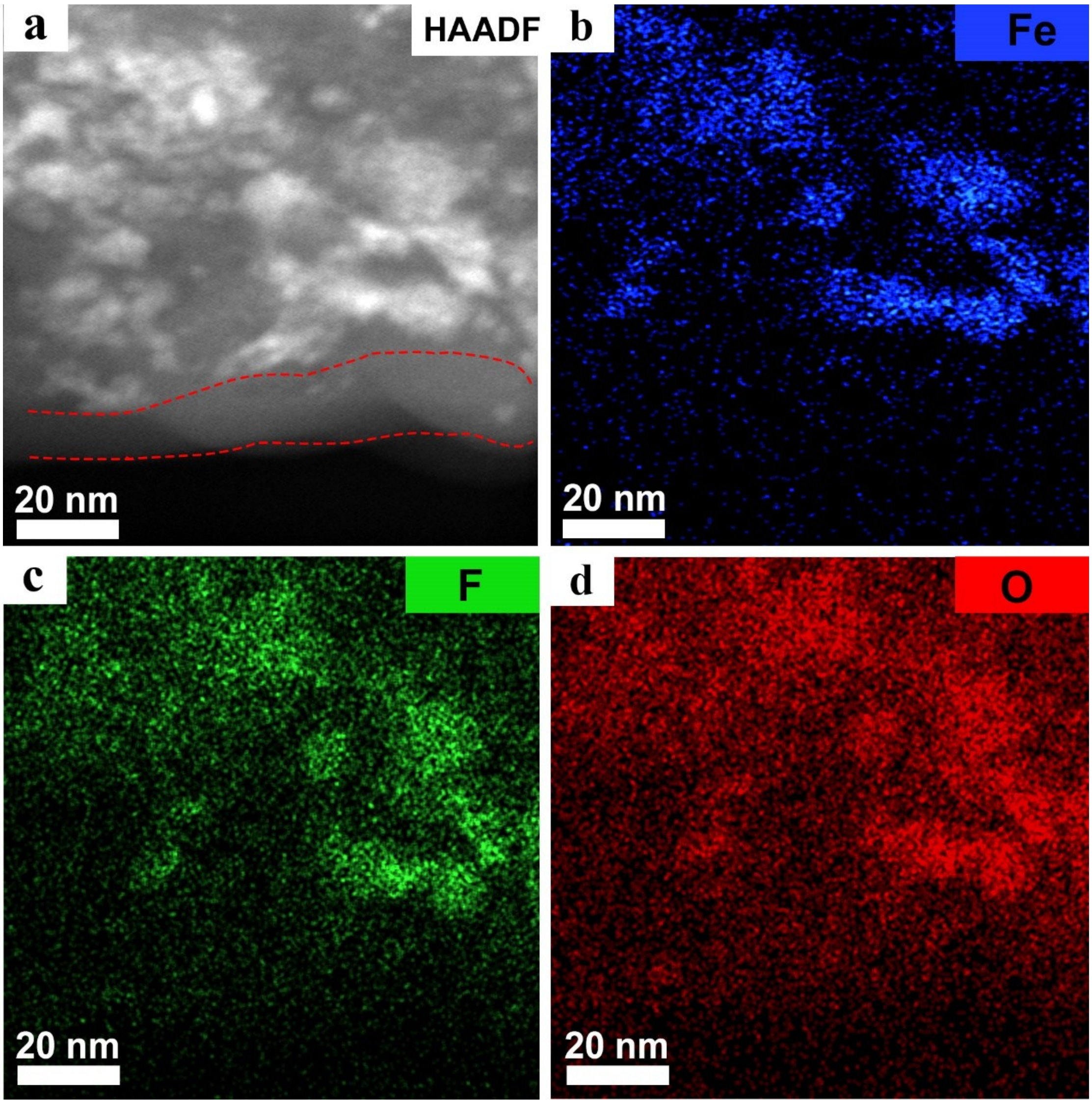

Supplementary Figure 14 | a, HAADF image and corresponding **b,** Fe, **c,** F and **d,** O mapping images of C@Fe_3C/Fe anode after cycling. The F mapping image is attributed to LiF, FeF_2 and FeF_3, and the O mapping image is attributed to Li_2O, Li_2CO_3 and polycarbonate (poly(CO_3)).

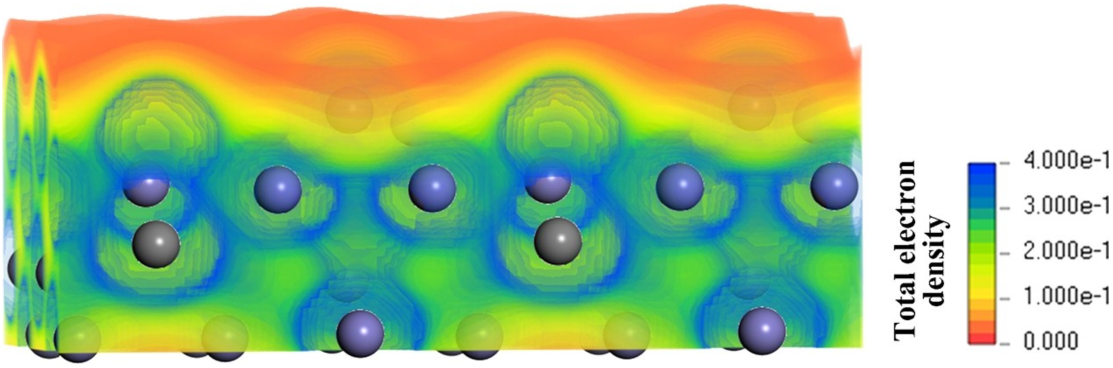

Supplementary Figure 15 | Electron density map of pristine Fe_3C.

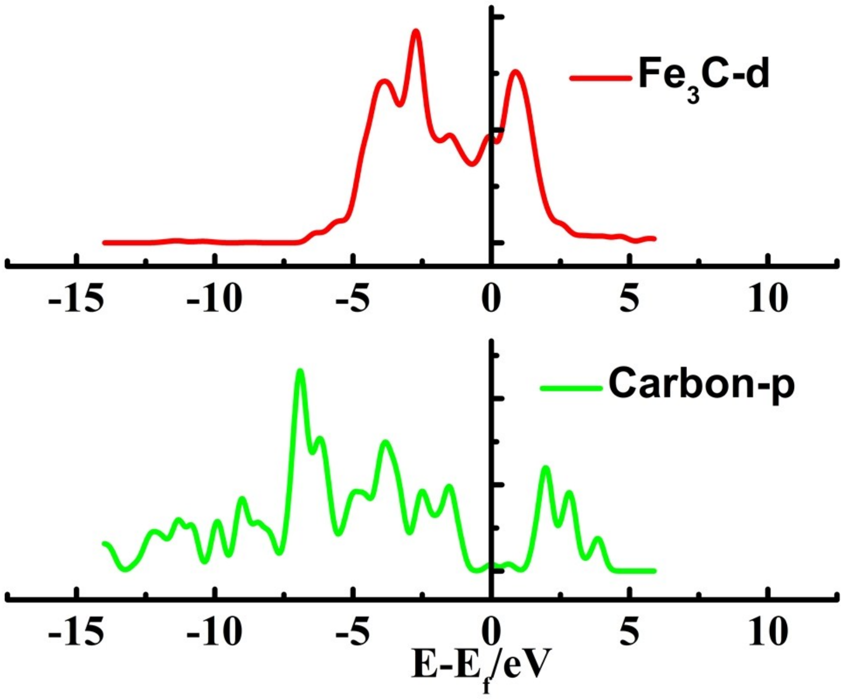

Supplementary Figure 16 | The PDOS comparison between carbon and Fe_3C.

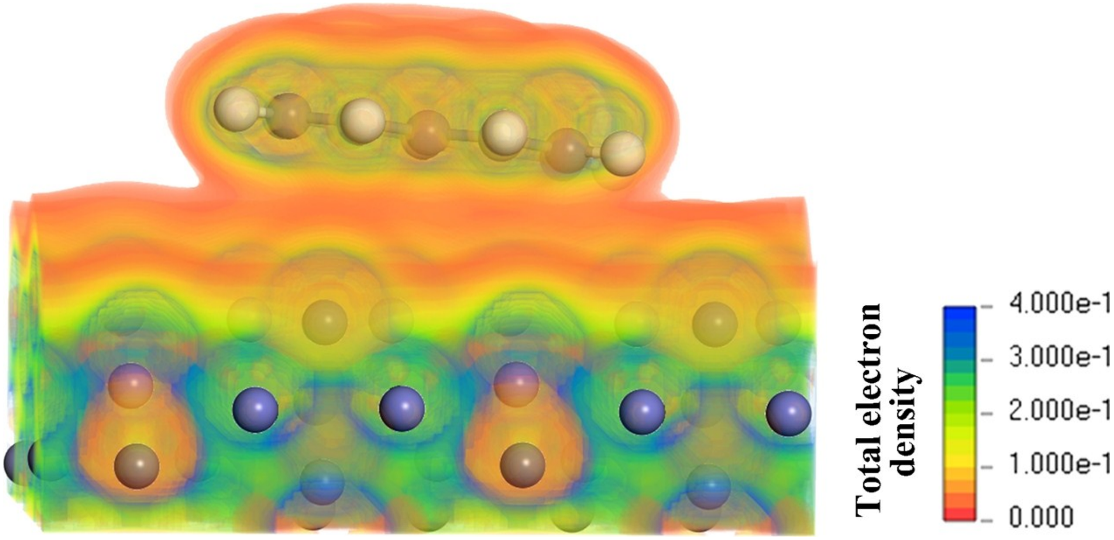

Supplementary Figure 17 | Electron density map of carbon on Fe_3C.

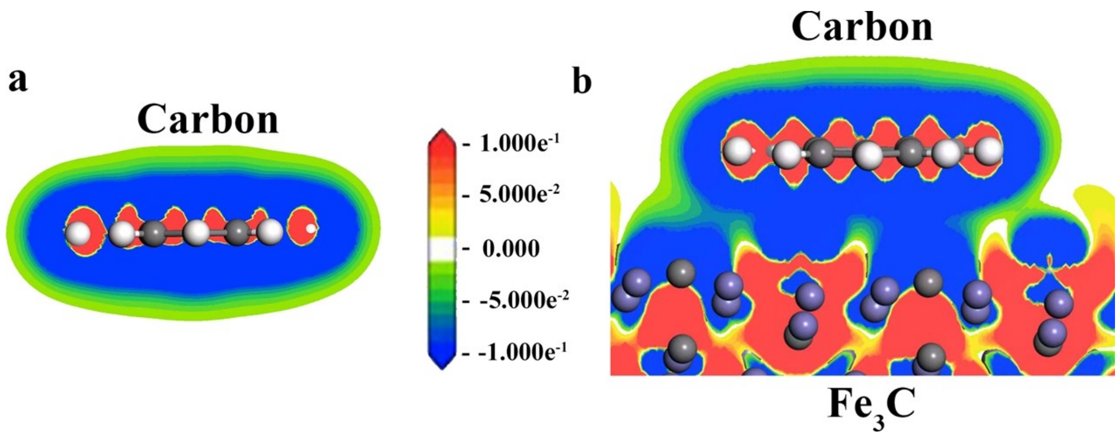

Supplementary Figure 18 | Electron density difference mapping for **a,** carbon and **b,** C@Fe_3C.

Red and blue regions indicate charge increase and decrease, respectively.

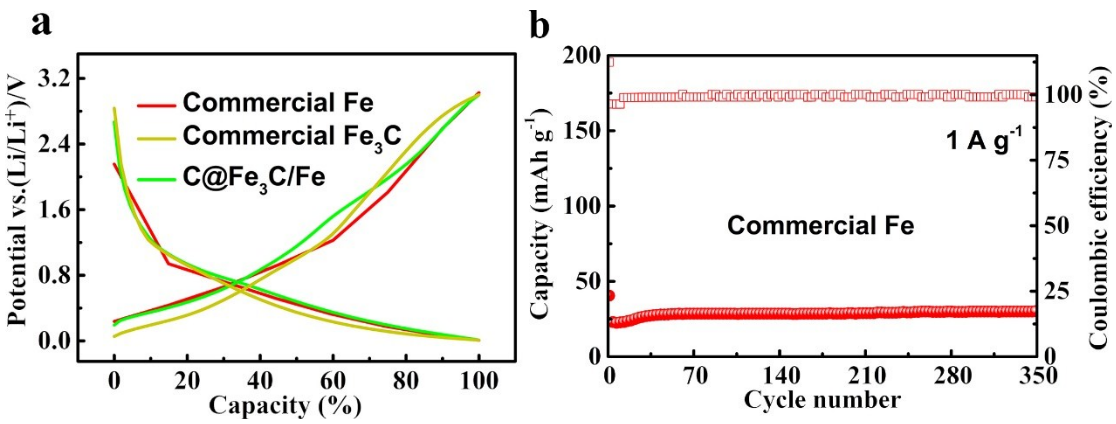

Supplementary Figure 19 | a, Charge/discharge profiles of commercial Fe, commercial Fe_3C and C@Fe_3C/Fe electrodes. The charge/discharge capacities are normalized for comparison. **b,** Cyclic performance of commercial Fe electrode.

Table 1

Table 1. Extra capacity phenomena of various materials and corresponding explanations

Composition	structure	Current density (mA g^{-1})	Cycles	capacity (mAh g^{-1})	Test conditions	explanations	Ref. No
α-Fe_2O_3	Hollow nanofibers	60	40	1293	1 M $LiPF_6$ +EC/DEC (1:1)	The formation of SEI film Lithium storage at the metal-Li_2O phase boundary constructed by iron particles	1
Co_3O_4	Single-crystalline nanobelts	100	60	980	1 M $LiPF_6$ +EC/DME (1:1)	Additional lithium storage in the grain boundaries of Li_2O and metal formed in the reduction cycle	2
Co_3O_4	Graphene-anchored nanoparticles	50	30	935	1 M $LiPF_6$ +EC/DMC (1:1)	The grain boundary area of the nanosized Co_3O_4 particles	3
MoS_2	1T(octahedral)	1000	800	~1800	1 M $LiPF_6$ +EC/DMC (6:4)	The generation of Mo atoms and its subsequent reversible reaction with Li to form Mo/Li_x	4
$CoCO_3$	Graphene-coated mesoporous	100	100	1070	1 M $LiPF_6$ +EC/DMC/EMC (1:1:1)	The reduction of Li_2CO_3 to Li_xC_2 with the formation of Li_2O	5

$FeCO_3$	Nanosized cube-like	200	130	761	1 M $LiPF_6$ +EC/DMC (1:1)	C^{4+} in CO_3^{2-} is reduced to C^0 or other low-valence C	6
N-doped graphene/ Fe-Fe_3C	Nanocomposite	1000	100	607	1 M $LiPF_6$ +EC/DMC/EMC (1:1:8)	The growth and decomposition of a polymer/gel-like film	7
Fe/Fe_3C-CNFs	Nanofibers	200	70	500	1 M $LiPF_6$ +EC/DMC/EMC (1:1:1)	The growth and decomposition of a polymer/gel-like film	8
N-Fe/Fe_3C@C	Nanomeshes	3600	500	819	1 M $LiPF_6$ +EC/EMC/DEC (4:3:3)	The growth and decomposition of a polymer/gel-like film	9
Fe-Fe_3C@rGO	Nanofibers	1500	200	558	1 M $LiPF_6$ +EC/DMC/EMC (1:1:1)	The growth and decomposition of a polymer/gel-like film	10
Fe@Fe_3C/C	Core-shell nanocomposites	50	30	~500	1 M LiPF6 +EC/DMC/EMC (1:1:1)	The growth and decomposition of a polymer/gel-like film	11

References:

[1] Chaudhari, S. & Srinivasan, M. 1D hollow α-Fe_2O_3 electrospun nanofibers as high performance anode material for lithium ion batteries. *Journal of Materials Chemistry.* **22**, 23049-23056 (2012).

[2] Huang, H., Zhu, W., Tao, X., Xia, Y., Yu, Z., Fang, J., Gan, Y. & Zhang, W. Nanocrystal-constructed mesoporous single-crystalline Co_3O_4 nanobelts with superior rate capability for advanced lithium-ion batteries. *ACS Applied Materials & Interfaces* **4**, 5974-5980 (2012).

[3] Wu, Z.-S., Ren, W., Wen, L., Gao, L., Zhao, J., Chen, Z., Zhou, G., Li, F. & Cheng, H.-M. Graphene anchored with Co_3O_4 nanoparticles as anode of lithium ion batteries with enhanced reversible capacity and cyclic performance. *ACS Nano* **4**, 3187-3194 (2010).

[4] Wang, L., Zhang, Q., Zhu, J., Duan, X., Xu, Z., Liu, Y., Yang, H. & Lu, B. Nature of extra capacity in MoS_2 electrodes: molybdenum atoms accommodate with lithium. *Energy Storage Mater.* **16**, 37-45 (2019).

[5] Ding, Z., Yao, B., Feng, J. & Zhang, J. Enhanced rate performance and cycling stability of a $CoCO_3$-polypyrrole composite for lithium ion battery anodes. *Journal of Materials Chemistry A* **1**, 11200-11209 (2013).

[6] Zhang, C., Liu, W., Chen, D., Huang, J., Yu, X., Huang, X. & Fang, Y. One step hydrothermal synthesis of $FeCO_3$ cubes for high performance lithium-ion battery anodes. *Electrochimica Acta* **182**, 559-564 (2015).

[7] Tan, Y., Zhu, K., Li, D., Bai, F., Wei, Y. & Zhang, P. N-doped graphene/Fe-Fe_3C nano-composite synthesized by a Fe-based metal organic framework and its anode performance in lithium ion batteries. *Chemical Engineering Journal.* **258**, 93-100 (2014).

[8] Li, J., Wen, W., Xu, G., Zou, M., Huang, Z. & Guan, L. Fe-added Fe_3C carbon nanofibers as anode for Li ion batteries with excellent low-temperature performance. *Electrochimica Acta* 153, 300-305 (2015).

[9] Zhou, J., Qian, T., Yang, T., Wang, M., Guo, J. & Yan, C. Nanomeshes of highly crystalline nitrogen-doped carbon encapsulated Fe/Fe_3C electrodes as ultrafast and stable anodes for Li-ion batteries. *Journal of Materials Chemistry A* **3**, 15008-15014 (2015).

[10] Joshi, B., Lee, J.-G., Samuel, E., Jo, H. S., Kim, T.-G., Swihart, M. T., Yoon, W. Y. & Yoon, S. S. Supersonically blown reduced graphene oxide loaded Fe-Fe_3C nanofibers for lithium ion battery anodes. *Journal of Alloys and Compounds* **726**, 114-120 (2017).

[11] Su, L., Zhou, Z. & Shen, P. Core-shell Fe@Fe_3C/C nanocomposites as anode materials for Li ion batteries. *Electrochimica Acta* **87**, 180-185 (2013).